Phase separation of a binary fluid containing surfactants in a Hele-Shaw cell

Jiunn-Ren Roan and E. I. Shakhnovich
Chemistry Department, Harvard University, 12 Oxford Street, Cambridge, Massachusetts 02138
(Received 13 July 1998)

The hydrodynamic effect on the phase separation of a two-dimensional binary fluid containing surfactants is studied. When the quench is deep, so that thermal fluctuations are ineffective, it is found that surfactant clusters tend to be trapped in domains of binary fluid when the hydrodynamic effect is included. The trapping of surfactant clusters, however, does not occur when the hydrodynamic effect is absent. It is also found that, contrary to the usual expectation, the domain grows with time algebraically at higher average surfactant concentrations and logarithmically at lower average surfactant concentrations. A simple scaling argument is given to explain this abnormal result. [S1063-651X(99)08402-0]

PACS number(s): 05.70.Fh, 64.10.+h, 62.20.Mk

I. INTRODUCTION

While the dynamics of phase separation in a binary system has been intensively studied [1–5], very little is known about the dynamics of phase separation in a ternary system made up of a binary fluid and surfactants such as microemulsions. A surfactant is typically composed of two parts, each being attracted to one component of the binary fluid. Examples are amphiphilic molecules (e.g., soap) in an oil-water mixture and *A*-*B* diblock copolymers in a blend of *A* and *B* homopolymers. The presence of surfactants in a phase-separating binary fluid significantly alters the dynamic as well as equilibrium properties of the fluid. Because of the interconnection of the two parts in the surfactant, the binary fluid cannot freely separate into two macroscopic domains, instead, it segregates into mesoscopic domains, with surfactants being located at the interfaces between domains, when thermal equilibrium is reached. The equilibrium domain structure depends on the composition of the ternary mixture. The morphology of these systems has been studied in great detail in the past decade [6], yet the study of the dynamics of phase separation in these systems has just started to attract more attention [7–12]. It is still unclear to what extent the hypothesis and theories developed for binary system can be applied to binary fluid–surfactant systems.

Several models have been proposed for amphiphilic systems. Gompper and Schick classified these models in terms of types of approach: microscopic, Ginzburg-Landau, and membrane approaches [6]. Since most theories on the dynamics of phase separation are constructed using the Ginzburg-Landau approach, it is convenient to use continuum models to study the dynamics of phase separation in amphiphilic systems. Models using this approach can be further classified in terms of the number of order parameters used. Usually the first order parameter describes the concentration difference between the two components in a binary fluid, the first additional order parameter describes the surfactant concentration, and so on. To make the description computationally economic while keeping minimum information regarding the surfactants so that one can see how the surfactants affect phase separation, two-order-parameter models perhaps are the most adequate models. Recently Komura and Kodama [10] proposed a two-order-parameter model which fixes the thermodynamic instability in the model proposed earlier by Laradji *et al.* [13]. They studied the dynamics of phase separation of their model at critical quench in the absence of a hydrodynamic effect [10] as well as in the presence of a steady shear flow [14]. However, it is known from the dynamic theory of phase separation in binary fluid that the hydrodynamic effect plays a crucial role [15]. For example, the domain growth exponent α, defined by the scaling of typical domain size $R(t)\sim t^{\alpha}$, changes from $\frac{1}{3}$ to 1 in three dimensions when the hydrodynamic effect is included. It is our purpose in this work to understand how the hydrodynamic effect changes the phase separation dynamics in Komura and Kodama's model.

The hydrodynamic effect has been customarily ignored in numerical studies of the phase separation dynamics of the binary fluid–surfactant system using the Ginzburg-Landau approach. To our knowledge, Pätzold and Dawson's work [16] is the only work that takes into account hydrodynamic effect in simulations. They applied the nonlinear hydrodynamics developed earlier [17] to the model proposed by Laradji *et al.* [13]. It was found that the domain grows algebraically when the thermal fluctuation is also included, and that the domain grows more slowly than logarithmically when the thermal fluctuation is not included. Instead of applying the approach developed in Ref. [17], here we shall adopt an alternative approach to incorporate hydrodynamics. Since our simulations will be performed in two dimensions, and since we believe that compressibility can be ignored without losing the essential feature of the hydrodynamic effect, we shall apply Navier-Stokes hydrodynamics and consider Hele-Shaw (HS) cell geometry to ensure that the system is quasi-two-dimensional and to enable us to ignore the inertia force [18,19]. Phase separation dynamics of binary fluid in a HS cell has been studied numerically in [20] using a cell dynamics system [21]. Although simple dimensional analysis gives $\alpha=\frac{1}{3}$ for the HS cell, the same as the growth exponent in systems without hydrodynamics, domains in the HS cell do grow faster. Therefore, faster domain growth is expected to be seen in ternary systems as well.

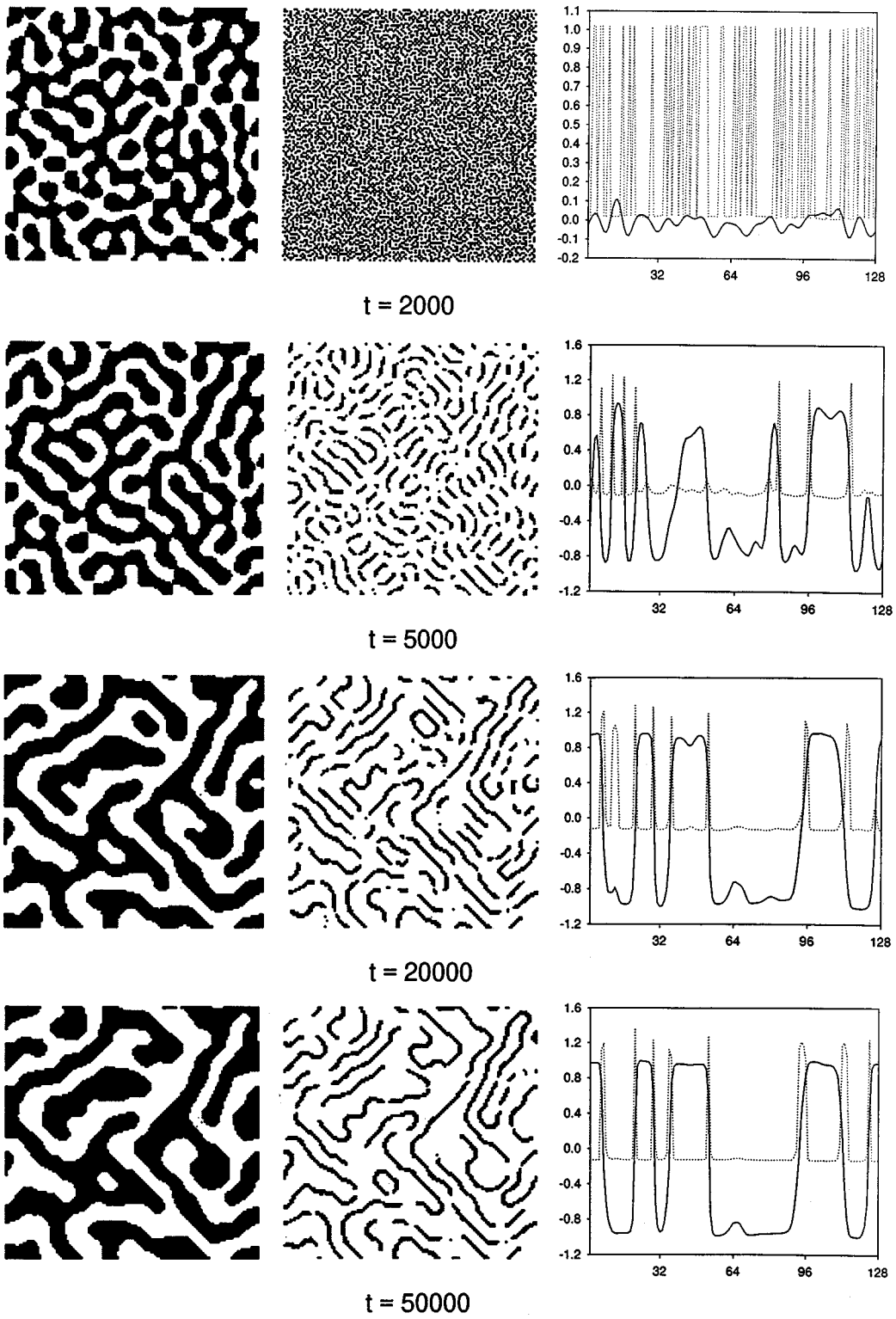

FIG. 1. Time evolution of ψ (left) and ρ (middle), and their profile (solid line for ψ and dotted line for ρ) along the [1,1] direction (right) for $\langle\rho\rangle = 0.1$ in an ordinary cell.

In Sec. II we define the model and dynamics, and outline the numerical scheme. In Sec. III we present and discuss the results of our simulations. Since surfactants reduce the interface tension which drives the motion of interfaces, it is expected that the system will appear less binary-fluid-like as the average surfactant concentration increases. However, our results seem to be in conflict with this expectation. A simple scaling argument will be given in this section to explain the observed time dependence of domain growth, which behaves more like a binary fluid at higher average surfactant concentrations. We shall also present a preliminary simulation in which both hydrodynamics and thermal fluctuations, which are ignored in the rest of simulations, are included. In Sec. IV, conclusions will be made.

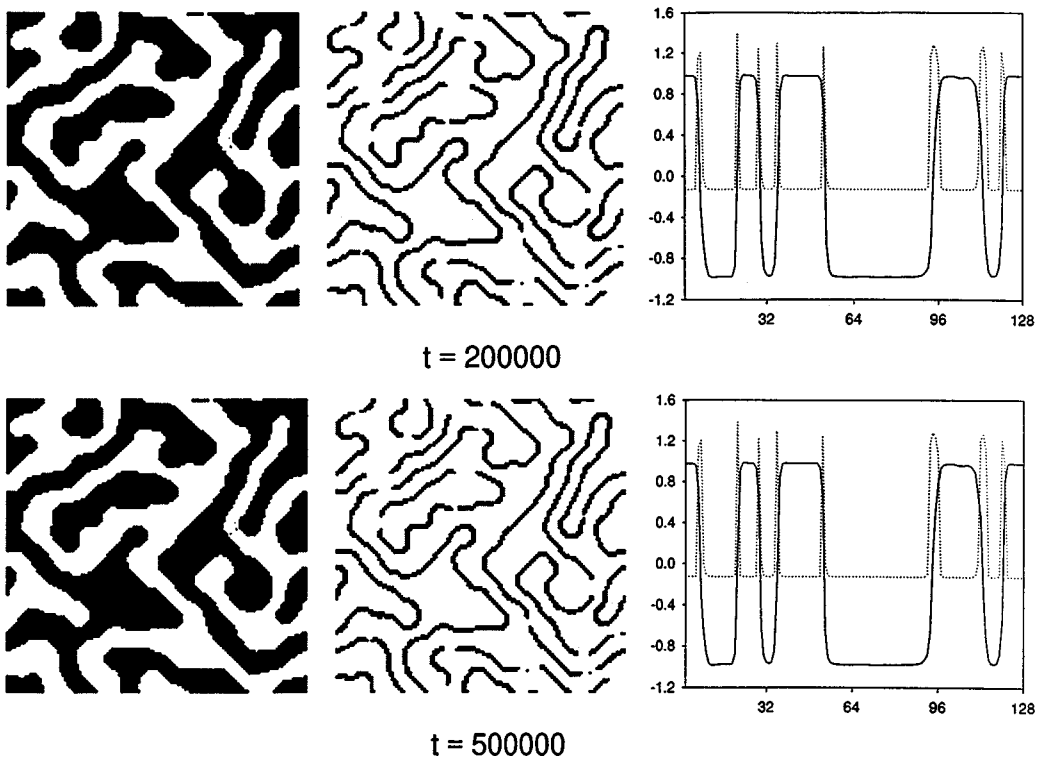

FIG. 1. (*Continued*).

II. MODEL

A. Free energy

The free energy proposed by Komura and Kodama is [10]

$$F=\int d\mathbf{r}[w(\nabla^2\psi)^2+d(\nabla\psi)^2-a\psi^2 +u\psi^4+e\rho^2(\rho-\rho_s)^2-s\rho(\nabla\psi)^2] \tag{2.1}$$

where $\psi(\mathbf{r},t)$ is the concentration difference between the two components of binary fluid and $\rho(\mathbf{r},t)$ is the surfactant concentration. Parameters w, d, a, u, e, ρ_s, and s are all positive. The free energy is bounded below by w and u terms. While the s term drives the surfactant to the interface between the two components, the e term makes the surfactant density tend to be either zero (far away from interfaces) or ρ_s (near interfaces). The terms d and a are the usual Ginzburg-Landau free energy terms which disfavor creation of interfaces and disordered phases, respectively. However, the effect of d is counteracted by s: Depending on the relative magnitude of d and $s\rho$, the creation of interfaces can be either energetically favorable or suppressed. Since in microemulsions the interface tension vanishes when the interface is saturated with surfactants [22], $d=s\rho_s$ will be chosen as in Ref. [10], so that creation of interfaces does not cost any energy when the local surfactant concentration is saturated, i.e., $\rho(\mathbf{r})=\rho_s$. The chemical potential needed to ensure conservation of order parameters ψ and ρ have been omitted, because the kinetic equations considered below always place these constant terms under the action of spatial differentiation.

Equation (2.1) has been used to model the dynamics of phase separation of binary fluid–surfactant mixture at critical quench in the absence of hydrodynamic effect [10] and in the presence of a steady shear flow [14]. The results of Ref. [10], in particular the behavior of domain growth, differ from the results obtained in the three-order-parameter model proposed by Kawakatsu and co-workers [7,23,24], in which the director of surfactant is used as the third order parameter. Komura and Kodama's model and Kawakatsu and co-workers' model may not belong to the same universal class.

B. Dynamics

Phase separation dynamics of the ternary system described by Eq. (2.1) is modeled by the kinetic equations [25,26]

$$\frac{\partial\psi(\mathbf{r},t)}{\partial t}+\mathbf{u}(\mathbf{r},t)\cdot\nabla\psi(\mathbf{r},t)=M_\psi\nabla^2\frac{\delta F}{\delta\psi(\mathbf{r},t)}+\eta_\psi(\mathbf{r},t) \tag{2.2a}$$

$$\frac{\partial\rho(\mathbf{r},t)}{\partial t}+\mathbf{u}(\mathbf{r},t)\cdot\nabla\rho(\mathbf{r},t)=M_\rho\nabla^2\frac{\delta F}{\delta\rho(\mathbf{r},t)}+\eta_\rho(\mathbf{r},t) \tag{2.2b}$$

$$\overline{\rho}\left[\frac{\partial\mathbf{u}(\mathbf{r},t)}{\partial t}+\mathbf{u}(\mathbf{r},t)\cdot\nabla\mathbf{u}(\mathbf{r},t)\right] =\overline{\eta}\nabla^2\mathbf{u}(\mathbf{r},t)-\nabla p(\mathbf{r},t)+\frac{\delta F}{\delta\psi(\mathbf{r},t)}\nabla\psi(\mathbf{r},t) +\frac{\delta F}{\delta\rho(\mathbf{r},t)}\nabla\rho(\mathbf{r},t)+\boldsymbol{\zeta}(\mathbf{r},t), \tag{2.2c}$$

where M_ψ and M_ρ are transport coefficients, $\overline{\rho}$ and $\overline{\eta}$ are the density and viscosity of the system [27], and η_ψ, η_ρ, and $\boldsymbol{\zeta}$

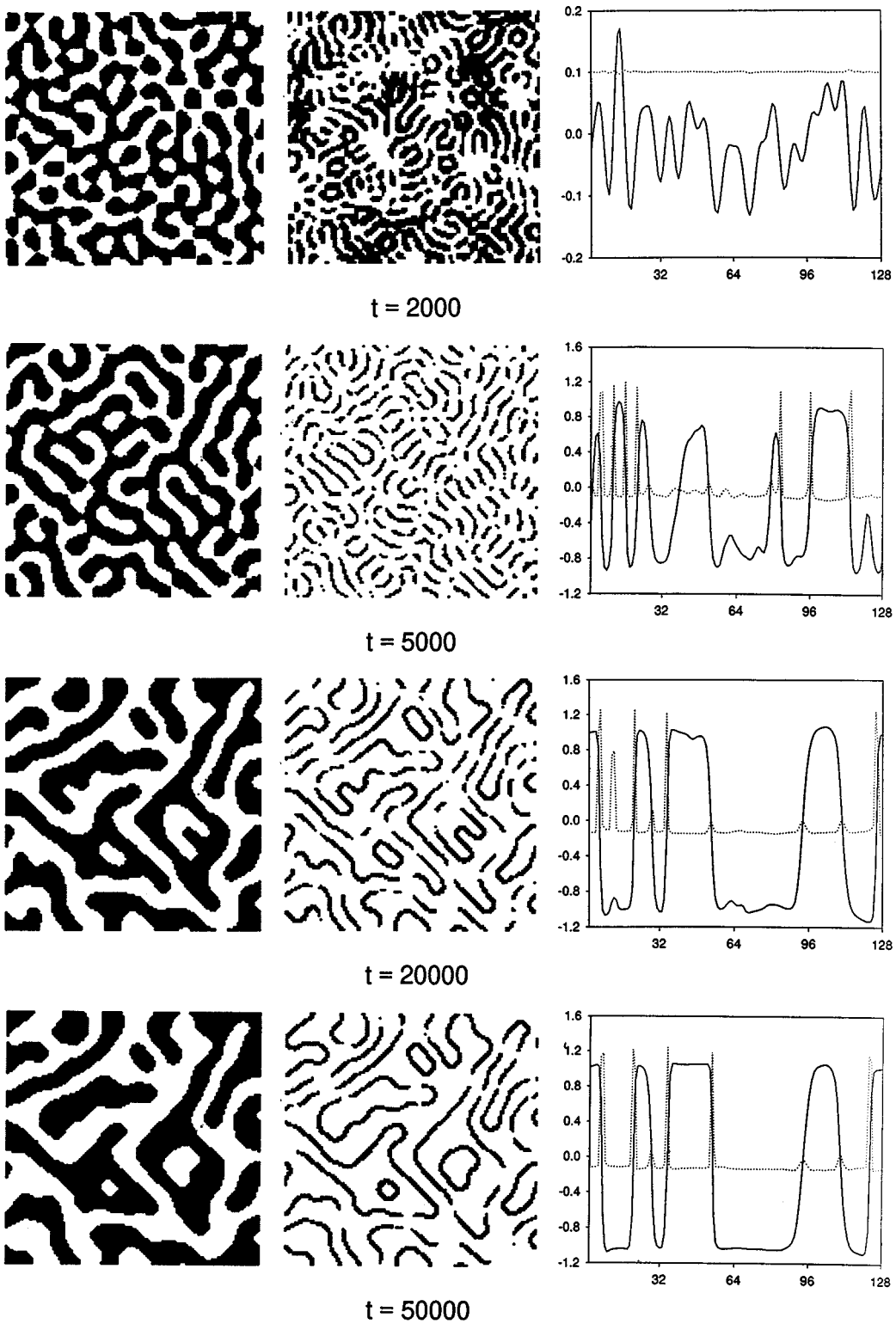

FIG. 2. Same as Fig. 1, for $\langle\rho\rangle = 0.1$ in a HS cell, starting from the same initial distributions of ψ and ρ as in Fig. 1.

are the thermal fluctuations satisfying fluctuation-dissipation relations for the corresponding fields. Equations (2.2) couple the usual Cahn-Hilliard-Cook equations [28,29] for conserved order parameters ψ and ρ to a Navier-Stokes equation whose stress tensor is properly modified by the coupling. It can be easily seen through the corresponding Fokker-Planck equation that an alternative form of the coupling terms in Eq. (2.2c) is

$$-\left[\nabla\frac{\delta F}{\delta\psi(\mathbf{r},t)}\right]\psi(\mathbf{r},t)-\left[\nabla\frac{\delta F}{\delta\rho(\mathbf{r},t)}\right]\rho(\mathbf{r},t). \qquad (2.3)$$

The statistical dynamics generated by this alternative form should be the same as what Eqs. (2.2c) describes.

In Eqs. (2.2) we have assumed that the system is incompressible. The phase separation dynamics in a compressible

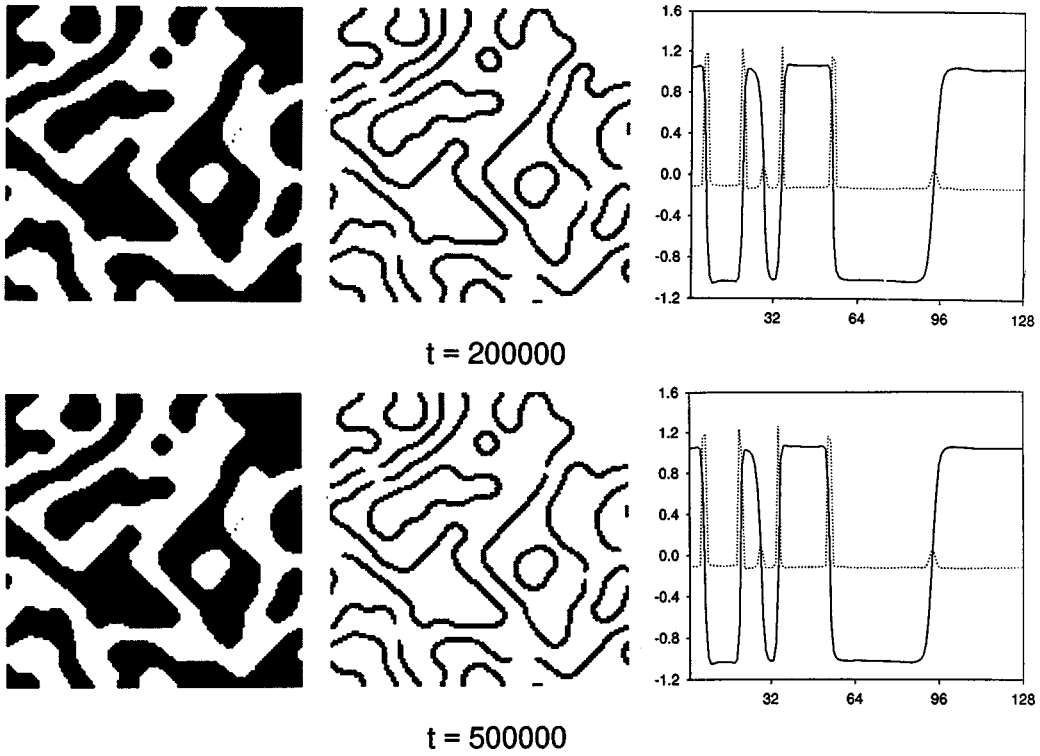

FIG. 2. (*Continued*).

ternary system was discussed in Ref. [16]. However, we believe that the compressibility does not significantly affect the behavior of phase separation as long as the system is far away from the critical regime.

To solve Eqs. (2.2) the following assumptions will be imposed in order to simplify simulations. We first assume that in the late stage thermal fluctuations are irrelevant, as far as the scaling of domain growth is concerned. The validity of this assumption has been numerically demonstrated for phase separation in binary systems [30,31]. As we will see in Sec. III, for the ternary system considered here, this assumption also holds in a very wide range of late stages. In this range the existence of well-separated domains with length scales much larger than the length scale of the fluctuation-induced raggedness should make the system become less globally affected by thermal fluctuations. Only in the very late stage does this assumption break down (see Ref. [16]. See also Sec. III D). Second, we shall assume that the fluid motion is slow enough so that the second order term $\mathbf{u}\cdot\nabla\mathbf{u}$ can be ignored (Stokes approximation). This is also reasonable because the collective motion of fluid is limited by the slow diffusion process in the absence of shear flows. Finally, we also assume that the relaxation of the fluid field is much faster than the relaxation of order paramerter fields (Markov approximation). This assumption is valid as long as the fluid is far from critical regime. With these assumptions, the kinetic equations become

$$\frac{\partial\psi(\mathbf{r},t)}{\partial t}+\mathbf{u}(\mathbf{r},t)\cdot\nabla\psi(\mathbf{r},t)=M_{\psi}\nabla^2\frac{\delta F}{\delta\psi(\mathbf{r},t)}, \quad (2.4a)$$

$$\frac{\partial\rho(\mathbf{r},t)}{\partial t}+\mathbf{u}(\mathbf{r},t)\cdot\nabla\rho(\mathbf{r},t)=M_{\rho}\nabla^2\frac{\delta F}{\delta\rho(\mathbf{r},t)}, \quad (2.4b)$$

$$0=\bar{\eta}\nabla^2\mathbf{u}(\mathbf{r},t)-\nabla p(\mathbf{r},t)+\frac{\delta F}{\delta\psi(\mathbf{r},t)}\nabla\psi(\mathbf{r},t)+\frac{\delta F}{\delta\rho(\mathbf{r},t)}\nabla\rho(\mathbf{r},t). \quad (2.4c)$$

To solve Eq. (2.4c) requires a properly specified boundary condition. Formally the solution is

$$\mathbf{u}(\mathbf{r},t)=\int d\mathbf{r}'\,\mathbf{T}(\mathbf{r}-\mathbf{r}')\cdot\left[\frac{\delta F}{\delta\psi(\mathbf{r}',t)}\nabla\psi(\mathbf{r}',t)+\frac{\delta F}{\delta\rho(\mathbf{r}',t)}\nabla\rho(\mathbf{r}',t)\right], \quad (2.5)$$

where $\mathbf{T}(\mathbf{r}-\mathbf{r}')$ is the Oseen tensor,

$$\mathbf{T}(\mathbf{r})=\int\frac{d\mathbf{k}}{(2\pi)^d}e^{i\mathbf{k}\cdot\mathbf{r}}\mathbf{T}_{\mathbf{k}}, \quad (2.6a)$$

$$\mathbf{T}_{\mathbf{k}}=\frac{g(k)}{\bar{\eta}}(\mathbf{1}-\hat{\mathbf{k}}\hat{\mathbf{k}}) \quad (2.6b)$$

(**1** being the unit tensor). The effect of the boundary condition enters through function $g(k)$ in Eq. (2.6b). The so-called free boundary condition gives the usual $g(k)=1/k^2$. Koga and Kawasaki [32] and Shinozaki and Oono [33] applied this form to study the phase separation in a binary fluid in three dimensions. In two dimensions, however, the free boundary condition leads to the well known Stokes paradox [19,34],

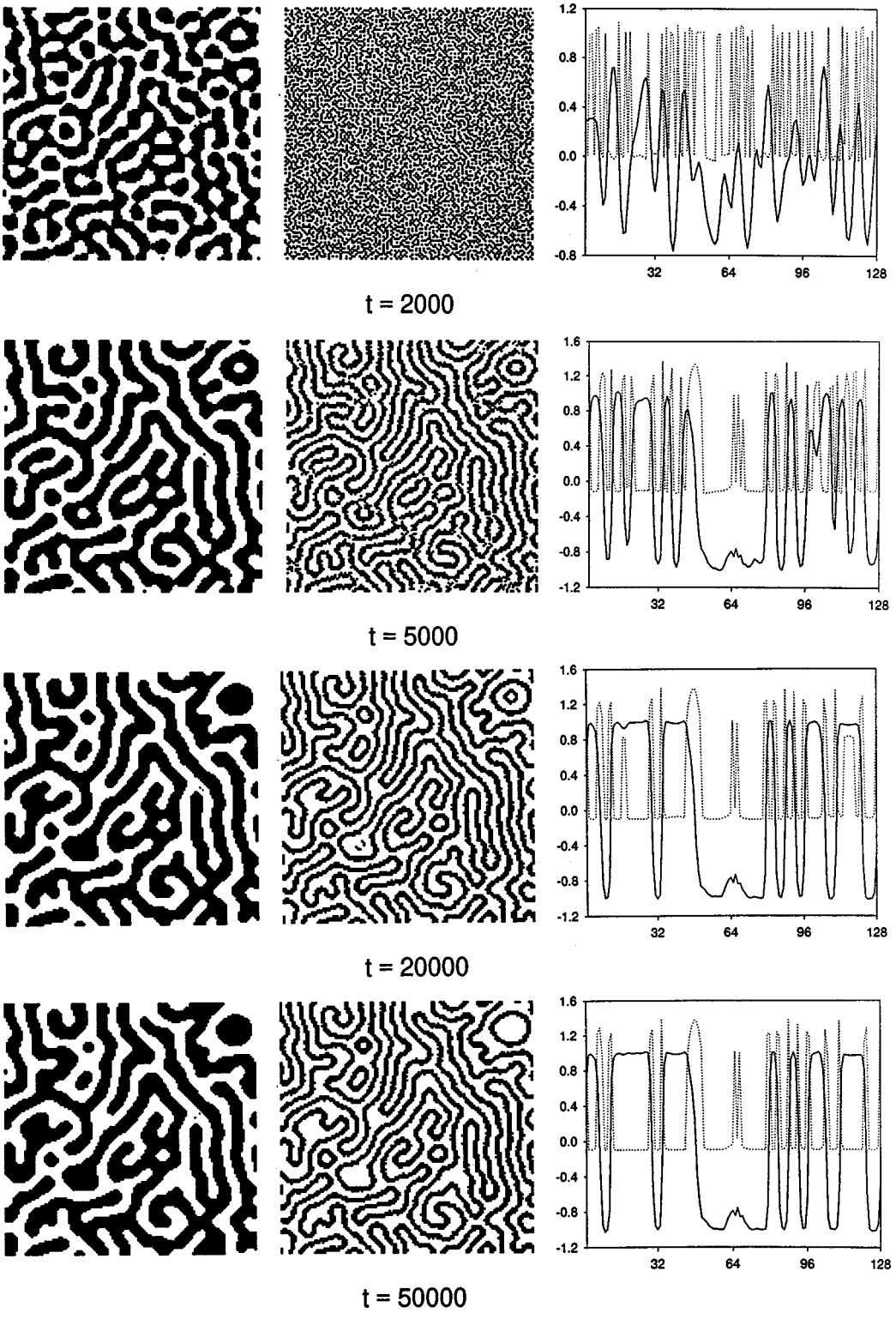

FIG. 3. Same as Fig. 1, for $\langle\rho\rangle = 0.4$ in an ordinary cell.

which is manifested by the logarithmic dependence of $\mathbf{T}(\mathbf{r})$. To avoid this unrealistic logarithmic dependence, we shall apply the no-slip boundary condition to incorporate the hydrodynamic effect in two dimensions. Experimentally this corresponds to the HS cell, in which the fluid is confined in two parallel narrowly separated plates [18,19]. With no-slip boundary condition, $g(k)$ becomes a constant and the Oseen tensor and fluid fields are given by

$$\mathbf{T}_{\mathbf{k}} = \frac{\overline{d^2}}{12\eta}(\mathbf{1} - \hat{\mathbf{k}}\hat{\mathbf{k}}), \tag{2.7}$$

$$\mathbf{u} = -\frac{\overline{d^2}}{12\eta}\left[\nabla p(\mathbf{r},t) - \frac{\delta F}{\delta\psi(\mathbf{r},t)}\nabla\psi(\mathbf{r},t) - \frac{\delta F}{\delta\rho(\mathbf{r},t)}\nabla\rho(\mathbf{r},t)\right],$$

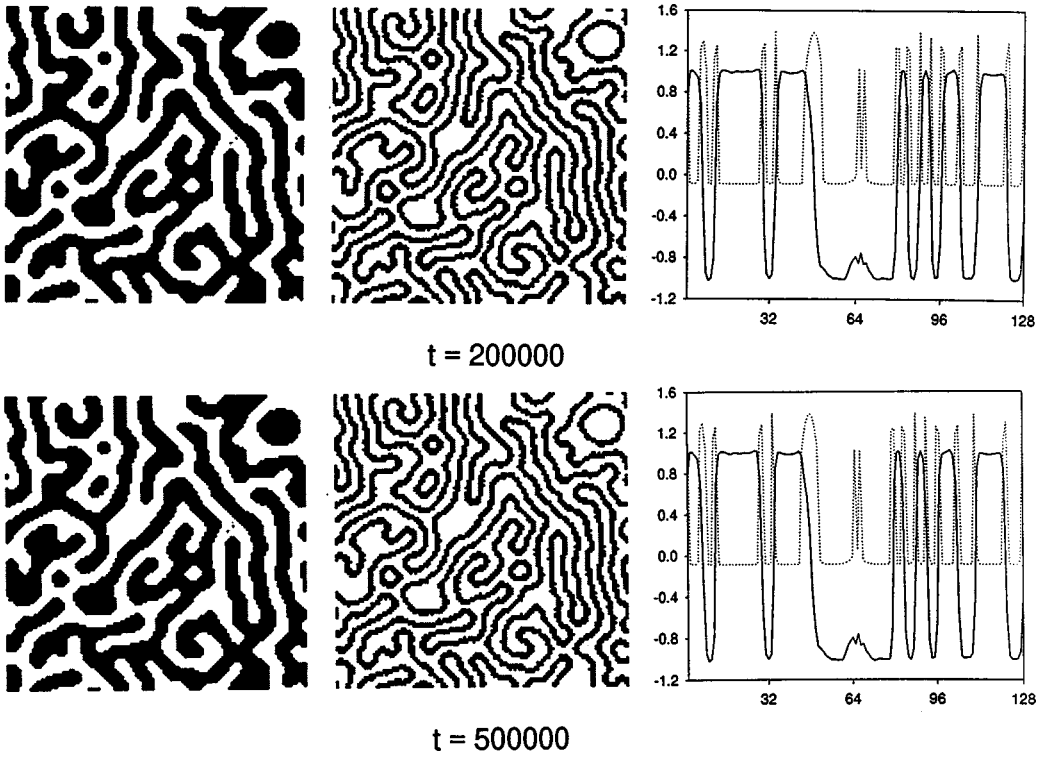

FIG. 3. (*Continued*).

where $\overline{d}$ is the spacing between the two plates. Equations (2.7) are sometimes called Darcy's law [19]. Since the parameters $\overline{d}$ and $\overline{\eta}$ do not enter the problem independently, we follow Shinozaki and Oono [20] and write

$$\mathbf{u}=-\frac{1}{c^2}\left[\nabla p(\mathbf{r},t)-\frac{\delta F}{\delta\psi(\mathbf{r},t)}\nabla\psi(\mathbf{r},t)-\frac{\delta F}{\delta\rho(\mathbf{r},t)}\nabla\rho(\mathbf{r},t)\right] \tag{2.8}$$

where $c^2>0$ is a parameter measuring the significance of the hydrodynamic effect. Products $M_\psi c^2$ and $M_\rho c^2$ give the relative contribution of diffusive effect to the hydrodynamic effect.

C. Numerical implementation: cell dynamic system

A cell dynamic system (CDS) [21] is used to solve the coupled kinetic equations (2.4a), (2.4b), and (2.8) numerically [10]. Following the CDS scheme for the hydrodynamic system proposed in Refs. [20,33], the CDS is implemented on a $L\times L$ square lattice $\mathbf{n}=(n_x,n_y)$ in the following order:

$$\mathcal{I}(\mathbf{n},t)=-A\tanh\psi(\mathbf{n},t)+\psi(\mathbf{n},t)+W(\tilde{\Delta})^2\psi(\mathbf{n},t)-(D-S\rho)\tilde{\Delta}\psi(\mathbf{n},t)+S\tilde{\nabla}\psi(\mathbf{n},t)\cdot\tilde{\nabla}\rho(\mathbf{n},t), \tag{2.9a}$$

$$\mathcal{J}(\mathbf{n},t)=E\rho(\rho-\rho_s)(2\rho-\rho_s)-\tfrac{1}{2}S(\tilde{\nabla}\psi(\mathbf{n},t))^2, \tag{2.9b}$$

$$\psi^*(\mathbf{n},t)=\psi(\mathbf{n},t)+M_\psi\tilde{\Delta}\mathcal{I}(\mathbf{n},t), \tag{2.9c}$$

$$\rho^*(\mathbf{n},t)=\rho(\mathbf{n},t)+M_\rho\tilde{\Delta}\mathcal{J}(\mathbf{n},t), \tag{2.9d}$$

$$p(\mathbf{n},t)=\mathcal{F}^{-1}\{[\nabla^2]_d^{-1}\mathcal{F}\tilde{\nabla}\cdot[\mathcal{I}(\mathbf{n},t)\tilde{\nabla}\psi(\mathbf{n},t)+\mathcal{J}(\mathbf{n},t)\tilde{\nabla}\rho(\mathbf{n},t)]\}, \tag{2.9e}$$

$$\mathbf{u}(\mathbf{n},t)=-\frac{1}{c^2}[\tilde{\nabla}p(\mathbf{n},t)-\mathcal{I}(\mathbf{n},t)\tilde{\nabla}\psi(\mathbf{n},t)-\mathcal{J}(\mathbf{n},t)\tilde{\nabla}\rho(\mathbf{n},t)], \tag{2.9f}$$

$$\psi(\mathbf{n},t+\Delta t)=\psi^*(\mathbf{n},t)-\tilde{\nabla}\cdot[\mathbf{u}(\mathbf{n},t)\psi^*(\mathbf{n},t)], \tag{2.9g}$$

$$\rho(\mathbf{n},t+\Delta t)=\rho^*(\mathbf{n},t)-\tilde{\nabla}\cdot[\mathbf{u}(\mathbf{n},t)\rho^*(\mathbf{n},t)], \tag{2.9h}$$

where $\mathcal{F}$ denotes Fourier transform and Δt the time step size used in obtaining the CDS from the original partial differential equations. (In the following, when time t is used, its unit will always be Δt.) The CDS parameters A, W, D, S, and E in Eqs. (2.9a) and (2.9b) are related to the free energy parameters in Eq. (2.1) by $A=1+2a\Delta t$, $W=2w\Delta t$, $D=2d\Delta t$, $S=2s\Delta t$, and $E=2e\Delta t$. The CDS discretization of the differential operators on a two-dimensional square lattice used are

$$\tilde{\nabla}\phi\equiv\frac{1}{2}[\phi(n_x+1,n_y)-\phi(n_x-1,n_y),\phi(n_x,n_y+1)-\phi(n_x,n_y-1)],$$

$$\tilde{\Delta}\phi\equiv\frac{1}{2}\sum_{\mathrm{NN}}\phi+\frac{1}{4}\sum_{\mathrm{NNN}}-3\phi,$$

$$[\nabla^2]_d\phi\equiv\sum_{\mathrm{NN}}\phi-4\phi,$$

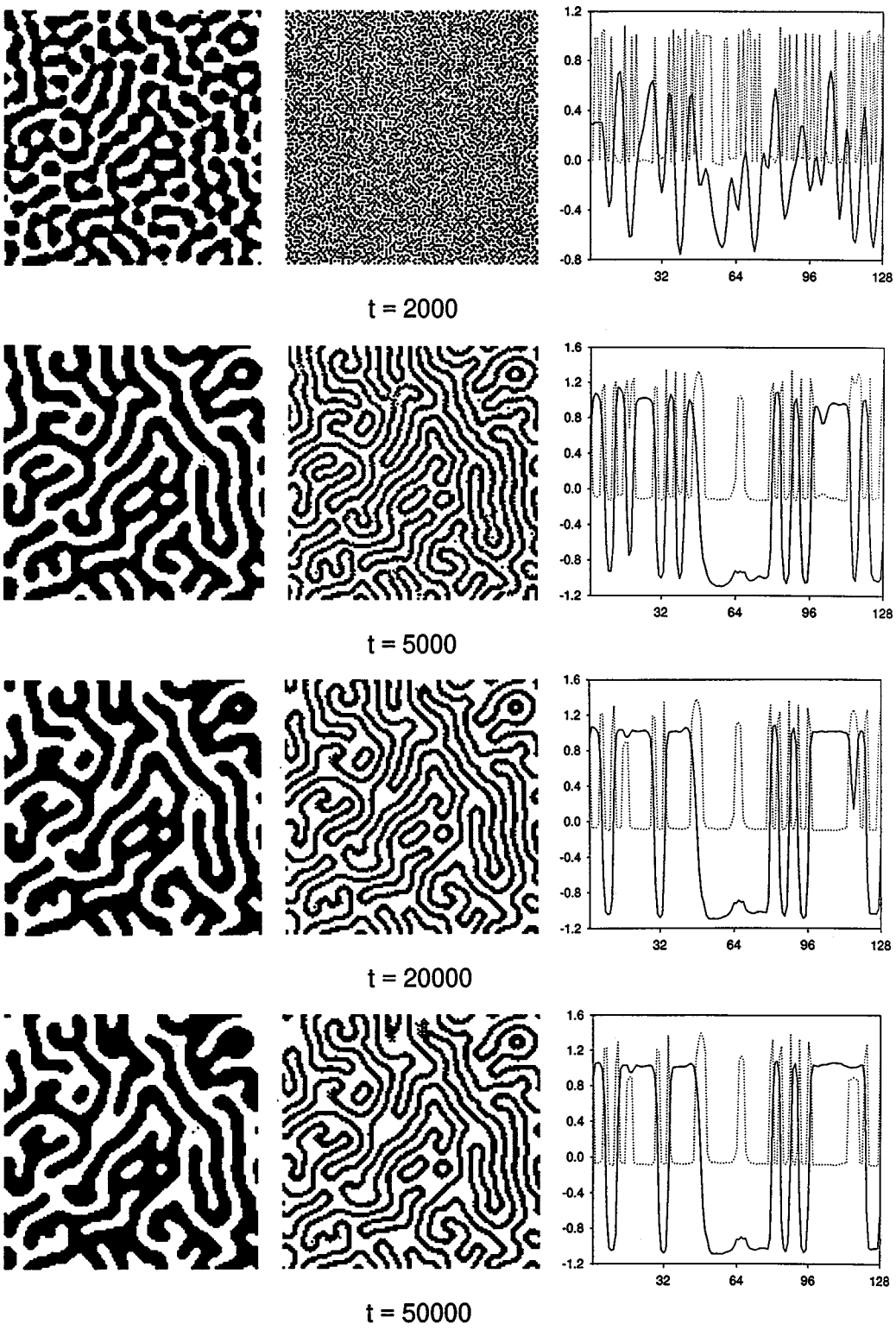

FIG. 4. Same as Fig. 1, for $\langle\rho\rangle=0.4$ in a HS cell, starting from the same initial distributions of ψ and ρ as in Fig. 3.

where NN and NNN are the nearest neighbor and next-nearest neighbor, respectively. Shinozaki and Oono, in Ref. [33], discussed the legitimacy of this hydrodynamic CDS scheme. We note that a similar scheme is also used in the calculations of quantum dynamics and femtochemical reactions [35].

In order to compare our result with Komura and Kodama's [10], their parameters are used in the following simulations: $L=128$, $A=1.3$, $W=0.2$, $D=0.5$, $S=0.5$, $E=0.25$, $\rho_s=1$, and $M_\psi=M_\rho=0.05$. The initial distributions of ψ and ρ will also follow their choice: random uniform distributions in $[-0.01,0.01]$ (critical quench) for ψ and $[\langle\rho\rangle-0.01,\langle\rho\rangle+0.01]$, where $\langle\rho\rangle$ is the average concentration of surfactants, for ρ. It is clear that the CDS scheme [Eqs. (2.9)] will suffer from numerical instability when c^2 is small while, on the other hand, large c^2 will render the hydrodynamic effect negligible. To see the hydrodynamic effect, therefore, we should use the smallest stable c^2 for the

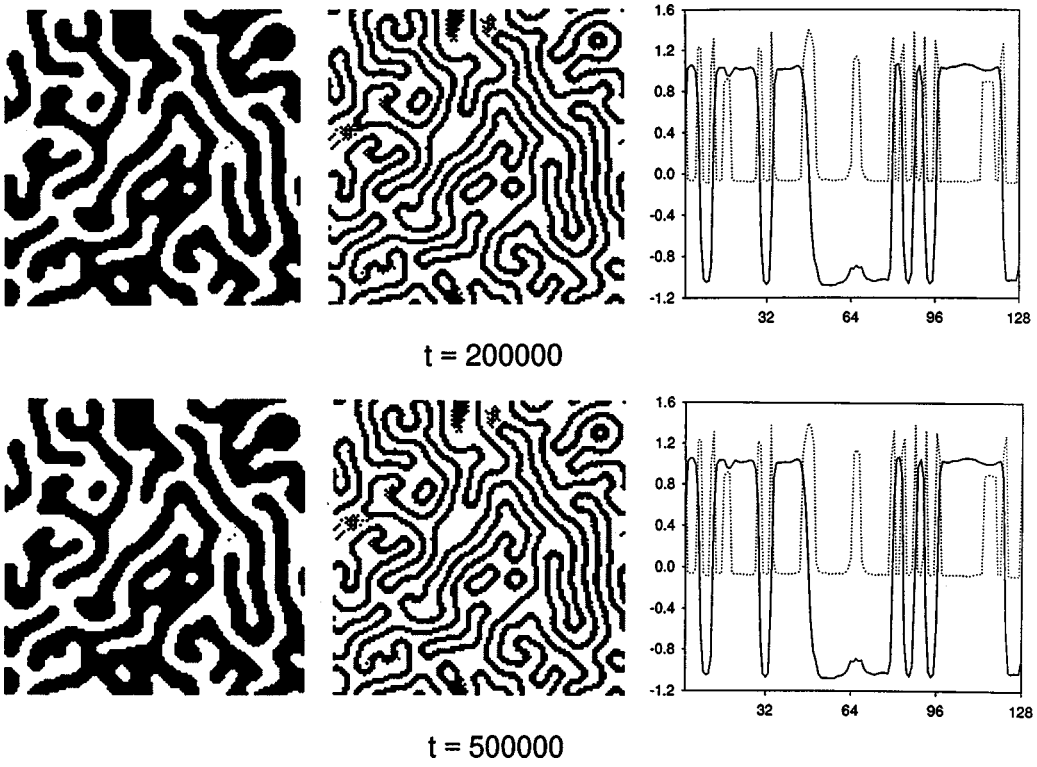

FIG. 4. (*Continued*).

chosen parameters. Since we find that $c^2=10$ gives a stable and significant hydrodynamic effect and $c^2=5$ leads to numerical overflow, $c^2=10$ is used in the following simulations.

III. RESULTS AND DISCUSSION

A. Time evolution of order parameters

Simulations are performed for $\langle\rho\rangle=0.1$, 0.2, 0.3, 0.4, and 0.5 over 500 000 time steps. Figures 1–4 show the typical time evolution of ψ and ρ in an ordinary cell (i.e., a cell without a hydrodynamic effect) and a Hele-Shaw cell. The structures shown in the left and middle columns of these figures are generated by darkening lattice sites where $\psi>0$ and $\rho>\langle\rho\rangle$, respectively (a ''hardened'' system [33]). Figures 5–7 show the final domain structures for $\langle\rho\rangle=0.2$, 0.3, and 0.5. There exists a percolation thershold of average surfactant density, above which the interfaces are everywhere saturated with surfactants when $t\rightarrow\infty$. These figures show that for our system this threshold is between $\langle\rho\rangle=0.2$ and $\langle\rho\rangle=0.3$ [36]. The most striking feature revealed in these figures is that above the percolation threshold there often exist clusters of trapped surfactants in domains of binary fluid in a Hele-Shaw cell. This can be understood as follows. The motion of surfactants is given by Eq. (2.4b), namely,

$$\frac{\partial\rho(\mathbf{r},t)}{\partial t}+\mathbf{u}(\mathbf{r},t)\cdot\nabla\rho(\mathbf{r},t)$$
$$=M_\rho\nabla^2[2e\rho(\rho-\rho_s)(2\rho-\rho_s)-s(\nabla\psi)^2]. \qquad (3.1)$$

In the early stage interfaces are not very sharp and the domain sizes are small, so surfactants are efficiently driven by the density gradient of binary fluid, $(\nabla\psi)^2$, and migrate over short distances, of the order of the domain sizes, to the nearby domain boundary. At the same time, the surfactant concentration ρ approaches its equilibrium values 0 or ρ_s, depending on whether the surfactant is located at the interface or in the domain. In the late stage, it is known that hydrodynamic convection dominates and helps the phase separation of the binary fluid proceed faster [15,20,37]. As the interfaces quickly withdraw, some of the surfactants that were located at the interfaces in early stage may lag behind and eventually find themselves being trapped deeply in domains, where the density gradient of ψ is almost zero. Since these surfactants have already evolved into $\rho=\rho_s$ in the early stage, and the slaved fluid field is also almost vanishing in the domain [cf. Eq. (2.7)], according to Eq. (3.1) the time evolution of these surfactants will be effectively frozen. On the other hand, in an ordinary cell the interface motion is slower, and surfactants have sufficient time to follow interfaces. Therefore, surfactants are usually not trapped. At lower $\langle\rho\rangle$, in early stage surfactants are unlikely to form large clusters, which would require longer times to diffuse to interfaces at later times, so trapped surfactants are less likely to be observed in these systems.

For the trapped surfactants the only way to reach interfaces is through thermal agitation. However, as we shall present below (Sec. III D), thermal fluctuations may not be effective enough until a very late stage, and some surfactants may be effectively trapped for a very long time. The trapping of surfactants, to our knowledge, has not been observed in previous simulations. It is interesting to pursue whether it is experimentally observable in deeply quenched systems.

B. Time evolution of characteristic length

Although domain structures in the HS cell are very similar to those in the ordinary cell, the domain growth behaves very differently. Following Shinozaki and Oono [33], the inverse characteristic length of the binary fluid is defined by

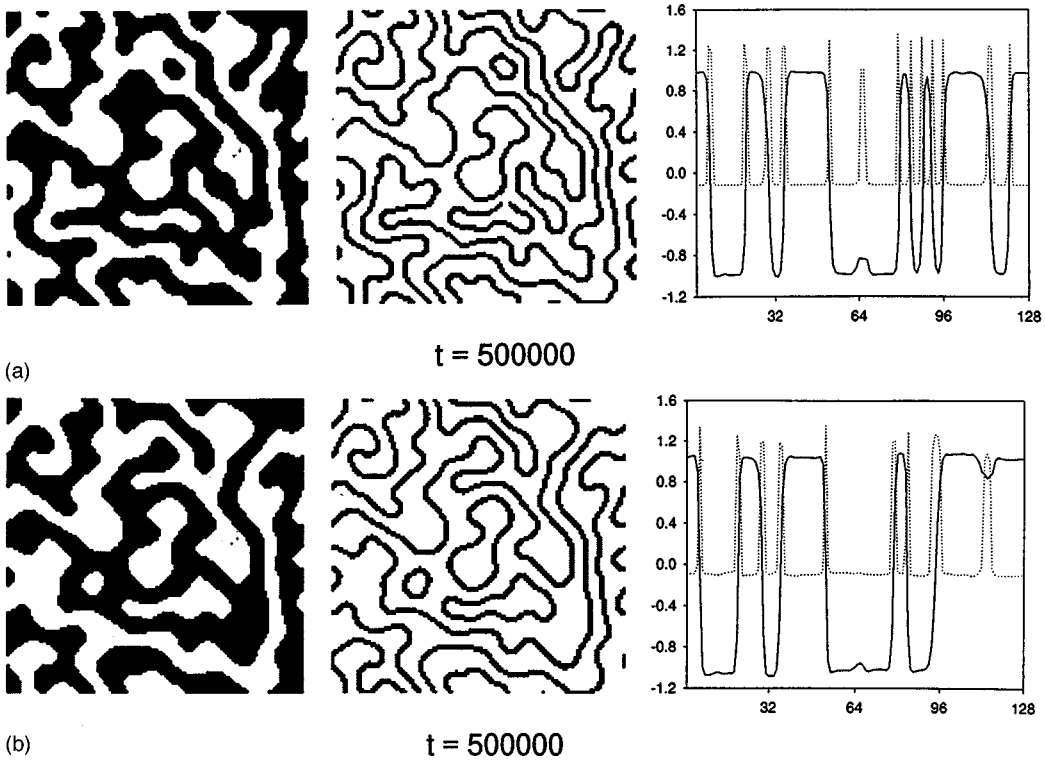

FIG. 5. Final patterns of ψ (left) and ρ (middle), and their profile (solid line for ψ and dotted line for ρ) along the [1,1] direction (right) for $\langle\rho\rangle=0.2$ in (a) an ordinary cell and (b) a Hele-Shaw cell. (a) and (b) have the same initial distributions of ψ and ρ.

$$\langle k_\psi(t)\rangle \equiv \frac{\sum_{\mathbf{k}\neq 0} |\mathbf{k}|^{-1} S_\psi(\mathbf{k},t)}{\sum_{\mathbf{k}\neq 0} |\mathbf{k}|^{-2} S_\psi(\mathbf{k},t)}, \tag{3.2}$$

where $S_\psi(\mathbf{k},t)\equiv\langle\psi_{\mathbf{k}}(t)\psi_{-\mathbf{k}}(t)\rangle$ is the structure factor of ψ. The inverse characteristic length of ρ can be similarly defined. The ensemble average in the definition of structure factor is obtained in this work by averaging over two samples [38]. Figure 8 shows the time evolution of $\langle k_\psi(t)\rangle$.

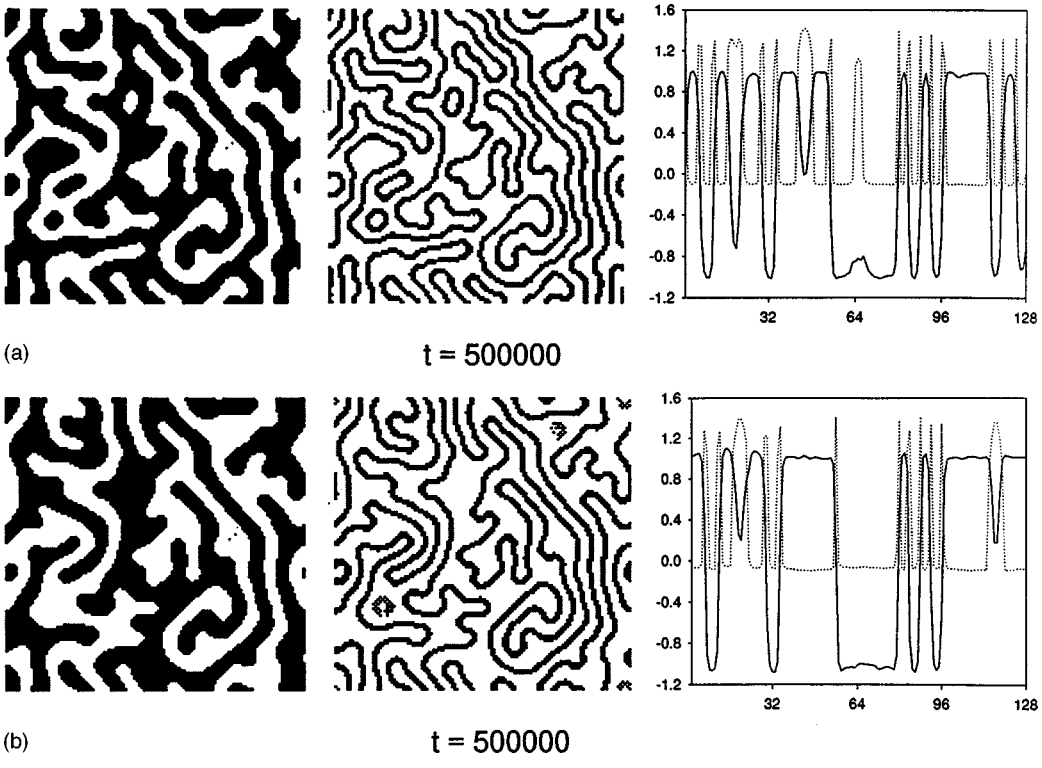

FIG. 6. Same as Fig. 5, for $\langle\rho\rangle=0.3$ in (a) an ordinary cell, and (b) a Hele-Shaw cell.

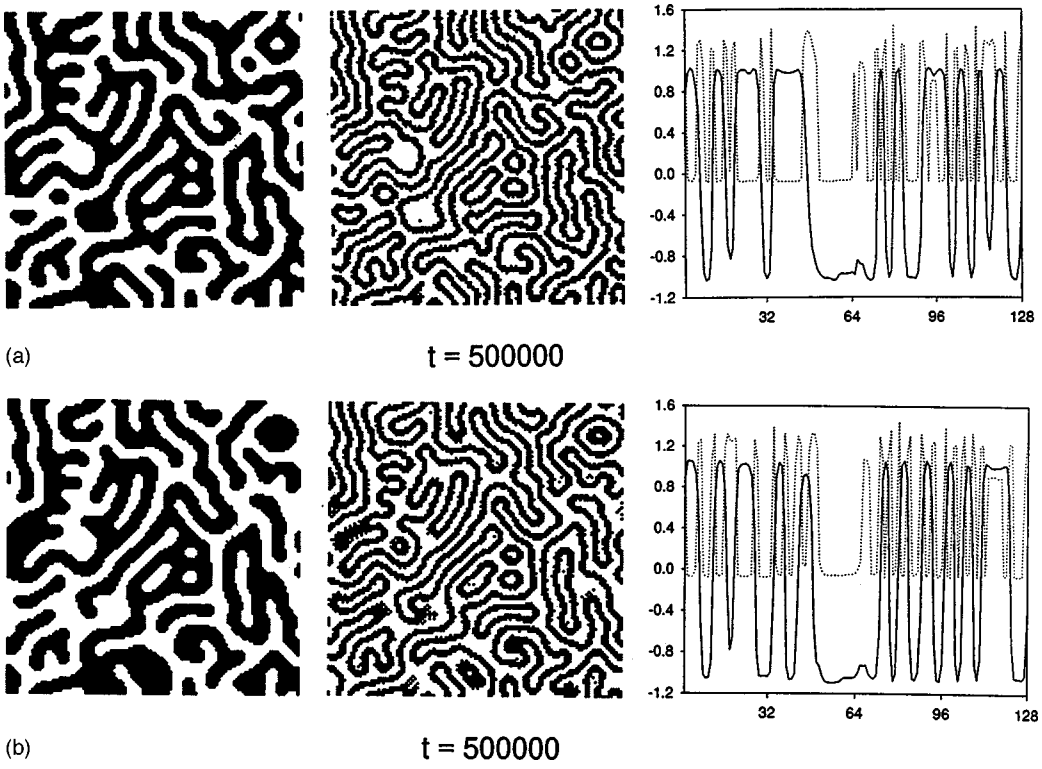

FIG. 7. Same as Fig. 5, for $\langle\rho\rangle = 0.5$ in (a) an ordinary cell, and (b) a Hele-Shaw cell.

Because thermal fluctuation is ignored, in early times there exists a plateau which signifies the Cahn-Hilliard linear regime [28]. Unlike the system introduced by Kawasaki and Kawakatsu [23], in which the linear regime is too short to be observed when surfactants are present [24], this plateau persists to the highest average concentration simulated. The linear regime, which is shorter at higher $\langle\rho\rangle$, ends around $t \approx 10^{3.5}$. This figure clearly shows that the domain grows faster in the HS cell than in an ordinary cell, as predicted in Refs. [15,20,37]. The difference between the two cells becomes more discernible after the linear regime ends. In the absence of thermal fluctuations, growth in both cells stops near the end of the simulation because the interface tension drops to zero when the interfaces are saturated with surfactants.

In Fig. 9 we plot the ratio of $\langle k_\rho\rangle$ to $\langle k_\psi\rangle$ versus time. This ratio can be used as an indication of how well the surfactants follow the motion of interfaces. If the surfactants closely follow the motion of interfaces, $\langle k_\rho\rangle/\langle k_\psi\rangle$ should be close to 2. Although $\langle k_\rho\rangle$ can be strongly biased by some small-scale trapped surfactants when the number of samples used in the ensemble average is small (for example, the curve for $\langle\rho\rangle = 0.4$ is biased toward a higher value because the system shown in Fig. 4 is one of the samples used in the ensemble average), it appears that all curves converge to the neighborhood of 2. The convergence sets in at the same time when the linear regime ends. This figure also implies that the percolation threshold lies between $\langle\rho\rangle = 0.2$ and 0.3. For $\langle\rho\rangle$ smaller than the percolation threshold, before surfactants on the interfaces become more evenly distributed by hydrodynamic convection in the late stage, surfactants are far less than enough to coat the interfaces and, therefore, they give smaller $\langle k_\rho\rangle$. For $\langle\rho\rangle$ greater than the threshold, in the early stage, surfactants, in addition to being able to coat the inter-

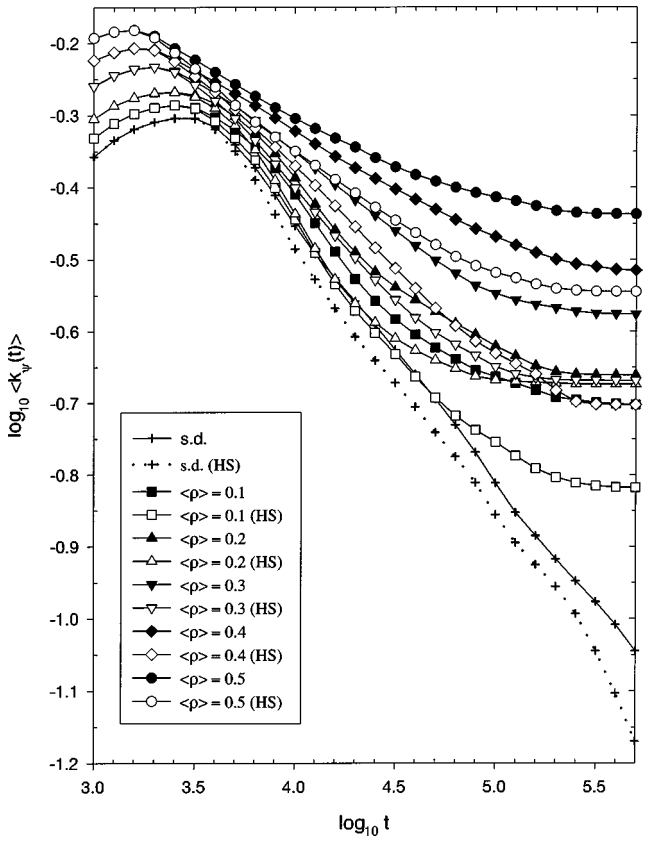

FIG. 8. Time evolution of the inverse characteristic length scale of ψ. s.d. represents spinodal decomposition of a binary fluid without surfactants.

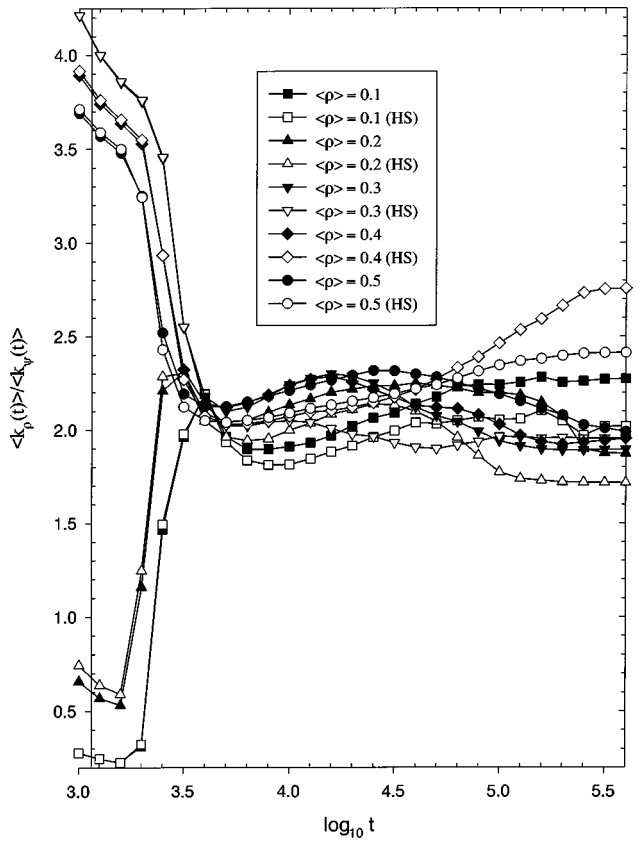

FIG. 9. Ratio of inverse characteristic length scales of the surfactant, $\langle k_\rho(t)\rangle$, and of the binary fluid, $\langle k_\psi(t)\rangle$.

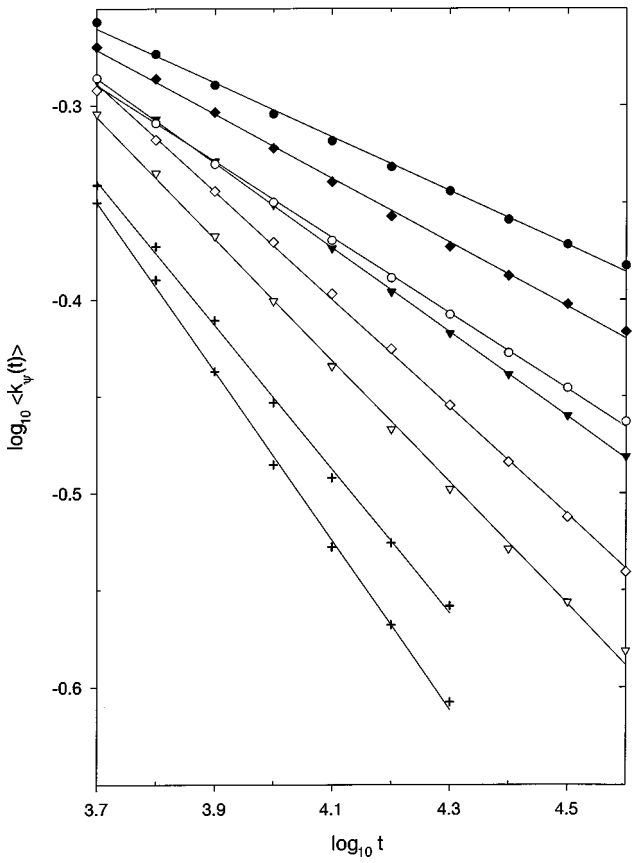

FIG. 10. Algebraic fit of the curves in Fig. 8. Symbols have the same meaning as those in Fig. 8, i.e., + with dotted line for $\langle\rho\rangle = 0.0$, etc. Points not used in the fit are not shown. Curves for $\langle\rho\rangle = 0.1$ and $\langle\rho\rangle = 0.2$ in both an ordinary cell and a HS cell cannot be fitted algebraically.

faces completely, are also able to scatter themselves in domains and make $\langle k_\rho\rangle$ greater.

Kawakatsu *et al.* argued in Ref. [24] that the characteristic domain size should grow algebraically and then, after the interfaces are saturated with surfactants, logarithmically. In Fig. 10 we fit the curves of Fig. 8 using an algebraic growth law $\langle k\rangle \sim t^\alpha$ [39]. In Fig. 11 the large t portions of these curves are fitted using a logarithmic growth law $\langle k\rangle \sim (\ln t)^\beta$ [39]. We find that, for $\langle\rho\rangle = 0.1$ and 0.2, neither ordinary nor HS cells can be fitted algebraically. The algebraic growth behavior may be too short to be observed for these cells. This seems to be inconsistent with the fact that these systems actually are more binary-fluid-like, in terms of amount of surfactants added, than systems with higher $\langle\rho\rangle$. A possible explanation is that the algebraic behavior seen in Fig. 10 is in fact logarithmic, because some curves in Fig. 10 can also be fitted by logarithmic law in a wider range of time. For example, the four curves for $\langle\rho\rangle = 0.4$ and 0.5 can be fitted logarithmically from $t = 10^{3.6}$ to $10^{5.4}$ (although the correlation coefficients are not as high as those found in Fig. 10.) In other words, it is possible that these curves have two logarithmic growth regimes. Nevertheless, since our purpose here is simply to demonstrate that the logarithmic behavior suggested prviously for other models [13,24] also gives reasonable fits for model (2.1), rather than to conclusively determine the growth law by simple fitting, we shall not pursue more precise fitting.

Instead, we discuss here a possible explanation for the inconsistency mentioned above. In Ref. [37], Kawasaki and Ohta apply drumhead model [40] to phase separation kinetics. The interface kinetic equation they derived is

$$\sigma K(a) - h(t)\Delta\psi_e = (\Delta\psi_e)^2 \int da' G(\mathbf{r}(a),\mathbf{r}(a'))v(a') - (\Delta\psi_e)^2 \int da'da'' G(\mathbf{r}(a),\mathbf{r}(a''))\mathbf{n}(a')\cdot\mathbf{T}(\mathbf{r}(a'),\mathbf{r}(a''))\cdot\mathbf{n}(a'')\sigma K(a''), \tag{3.3}$$

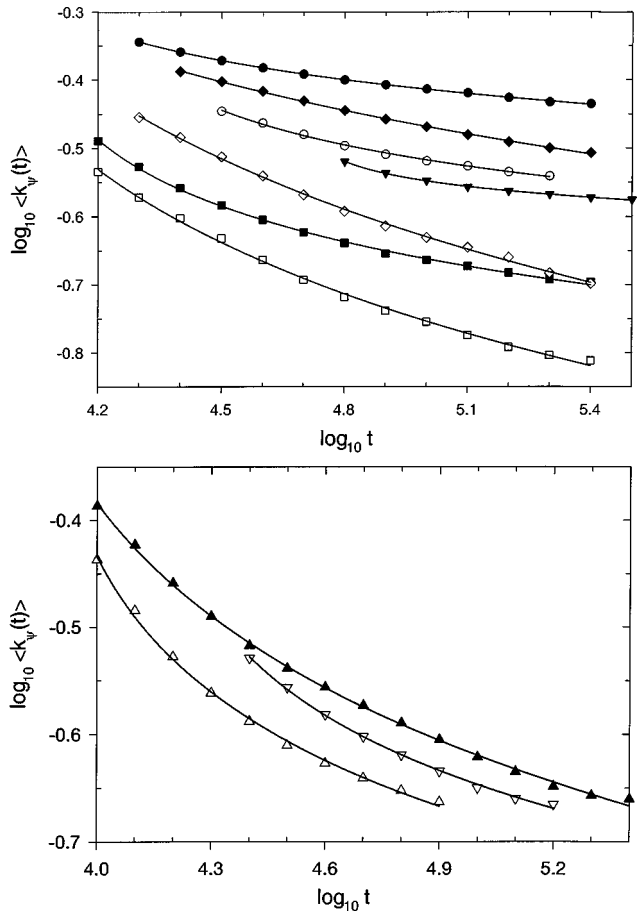

FIG. 11. Logarithmic fit of the curves in Fig. 8. The symbols have the same meaning as those in Fig. 8, i.e., + with dotted line for $\langle\rho\rangle=0.0$, etc. In order to make curves more distinguishable, they are arbitrarily separated into two plots. Points not used in the fit are not shown. Note that the times covered by the fit extend into the late part of the times used in algebraic fit (Fig. 10).

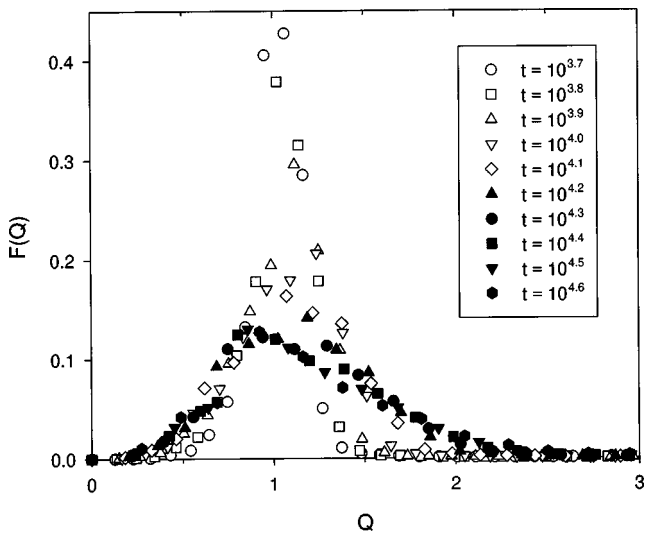

FIG. 12. Plot of scaled structure factor $F(Q)=\langle k\rangle^2 S(k)$ vs the scaled wave vector $Q=k/\langle k\rangle$ for $\langle\rho\rangle=0.1$ in a Hele-Shaw cell for times within the ''algebraic growth regime'' defined by Fig. 10. Filled symbols (including the symbol +) represent times that are also within the early ''logarithmic growth regime'' defined by Fig. 11).

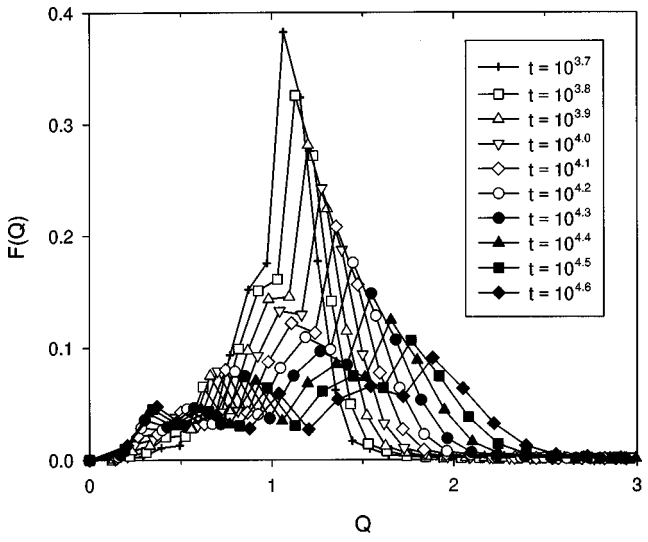

FIG. 13. Same as Fig. 12, for $\langle\rho\rangle=0.4$ in a Hele-Shaw cell.

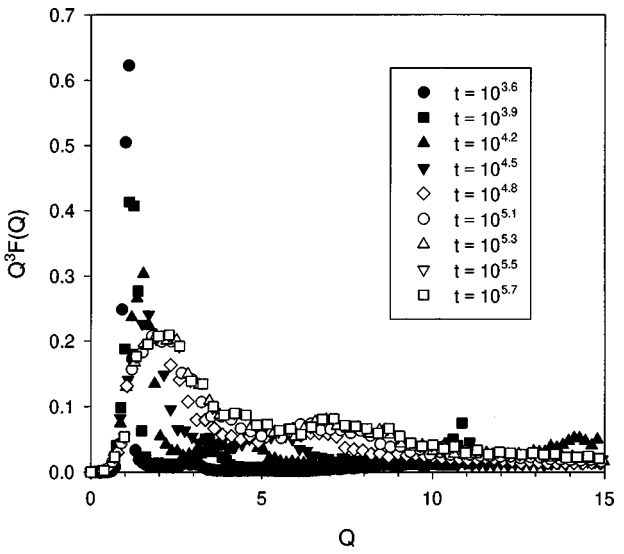

FIG. 14. Porod's plot for $\langle\rho\rangle=0.1$ in a Hele-Shaw cell for various times.

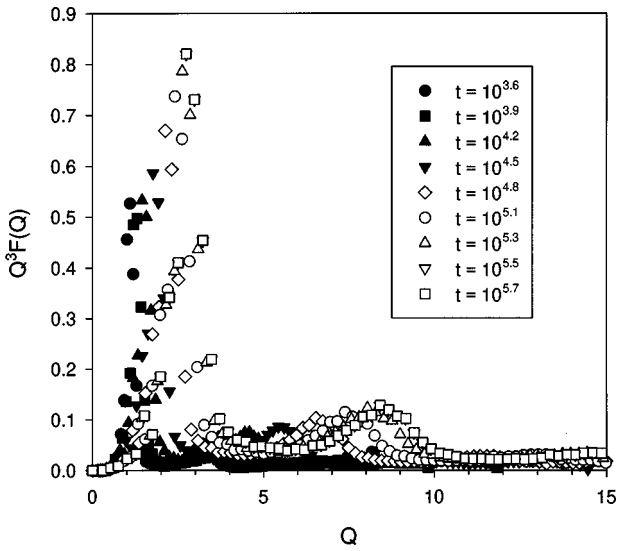

FIG. 15. Porod's plot for $\langle\rho\rangle=0.4$ in a Hele-Shaw cell for various times.

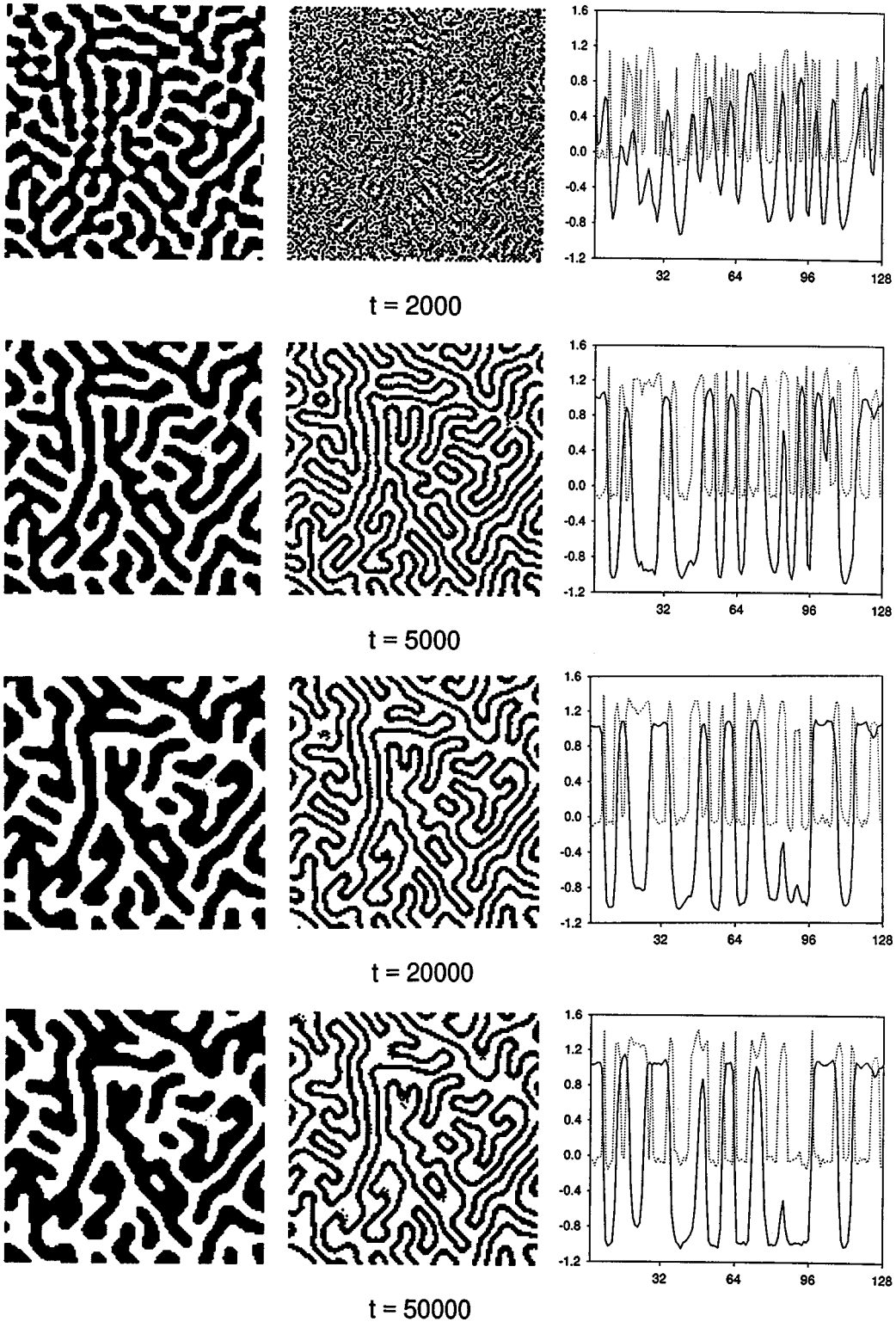

FIG. 16. Time evolution of ψ (left) and ρ (middle), and their profile (solid line for ψ and dotted line for ρ) along the [1,1] direction (right) for $\langle\rho\rangle=0.4$ in a thermally fluctuated Hele-Shaw cell, starting from the same initial distributions of ψ and ρ as Fig. 3.

where σ is the interface tension, $K(a)$ the mean curvature at a, a point on the interface; $h(t)$ an auxiliary function to be determined by conservation law; $\Delta\psi_e$ the difference between the two equilibrium ψ values; $v(a)$ the interface speed at a alone $\mathbf{n}(a)$, the unit normal vector to the interface at a pointing from domain with $\psi<0$ to $\psi>0$; and $G(\mathbf{r},\mathbf{r}')$ the solution of

$$M_\psi \nabla^2 G(\mathbf{r},\mathbf{r}') = -\delta(\mathbf{r}-\mathbf{r}'). \tag{3.4}$$

Following the argument in Refs. [37] and [24], in a Hele-Shaw cell, if a single characteristic length scale $R(t)$ dominates the phase separation, Eq. (3.3) gives, for a droplet of radius $R(t)$,

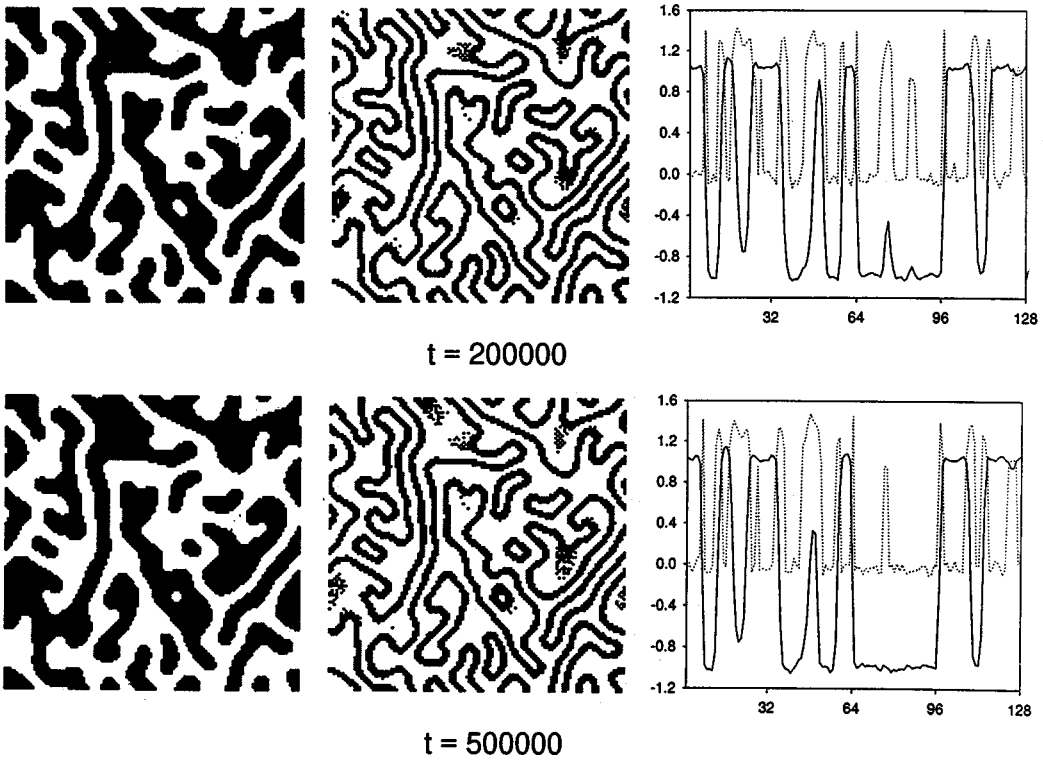

FIG. 16. (*Continued*).

$$\frac{\sigma}{R}\sim\frac{1}{R}\frac{dR}{dt}-\omega\frac{1}{R^2}\frac{\sigma}{R}, \tag{3.5}$$

where $h(t)$ is ignored for simplicity, and ω measures the importance of hydrodynamic effect. Therefore,

$$\frac{d}{dt}R(t)\sim\sigma\left(1+\frac{\omega}{R^2}\right). \tag{3.6}$$

The interface tension in Eq. (3.6) is a function of local surfactant concentration ρ. It can be estimated from Eq. (2.1) that $\sigma\sim\sqrt{d-s\rho}$ in the drumhead limit [40]. (For simplicity, we consider only $d>s\rho$.) Meanwhile, the local surfactant concentration ρ is inversely proportional to $R(t)$ in two dimensions, $\rho\sim\langle\rho\rangle/R$. These give

$$\frac{d}{dt}R(t)\sim\sqrt{\xi-\frac{\langle\rho\rangle}{R}}\left(1+\frac{\omega}{R^2}\right), \tag{3.7}$$

where $\xi>0$. If surfactants are not present, Eq. (3.7) gives the usual $R(t)\sim t^{1/3}$ law [5,20], when hydrodynamics is dominant. On the other hand, if there are surfactants, the solution of Eq. (3.7) gives

$$t\sim\{\text{linear combination of }\langle\rho\rangle^{(5-2m)/2}R^m\sqrt{\xi R-\langle\rho\rangle}\ \text{and}\ \langle\rho\rangle^3\ln[\sqrt{\xi R}+\sqrt{\xi R-\langle\rho\rangle}]\}, \tag{3.8}$$

where $2m=1$, 3, and 5 when hydrodynamics dominates, and

$$t\sim\{\text{linear combination of }R^{1/2}\sqrt{\xi R-\langle\rho\rangle}\ \text{and}\ \langle\rho\rangle\ln[\sqrt{\xi R}+\sqrt{\xi R-\langle\rho\rangle}]\}, \tag{3.9}$$

when the hydrodynamics is ineffective.

Although Eq. (3.8) still reduces to the $\frac{1}{3}$ law when $\langle\rho\rangle\rightarrow 0$, there is no guarantee that the binary-fluid-like behavior can be seen at intermediate $\langle\rho\rangle$, nor does it, given the complex form of Eq. (3.8), eliminate the possibility that the behavior of systems with higher $\langle\rho\rangle$ will appear to be more binary-fluid-like. Note that, while Eq. (3.3) is quite universal, the estimation of interface tension σ is tricky. Kawakatsu *et al.* [24] used an exponential form as their estimation and, therefore, lead to logarithmic growth law. As we noted above, logarithmic behavior may not be very distinct from algebraic behavior. Hence it is quite possible that the logarithmiclike behavior observed in Refs. [13,24] is indeed a delicate manifestation of the linear combination in Eq. (3.9). If the growth follows Eqs. (3.8) or (3.9), fitting $\ln\langle k\rangle-\ln t$ plot using a simple relationship such as an algebraic or logarithmic expression may not be meaningful. Furthermore, Eqs. (3.9) and (3.8) are derived based on the assumption that a single length scale dominates the system. As will be shown in Sec. III C, this may not be the case. If this assumption does not hold, the growth of the domain size will be more complicated than Eqs. (3.9) and (3.8).

Finally, note that the characteristic length scales in ordinary cells at the end of our simulations are consistent with the expectation that the more surfactants there are, the smaller the equilibrium domain sizes will be. This expectation, however, is not observed in HS cells without thermal fluctuations (Fig. 8). Neither was it observed in ordinary cells with thermal fluctuations [10]. Whether this expectation holds when both hydrodynamics and thermal fluctuations are included in model (2.1) needs further investigation.

C. Time evolution of structure factor and Porod's plot

The circularly averaged structure factor for the binary fluid is defined as

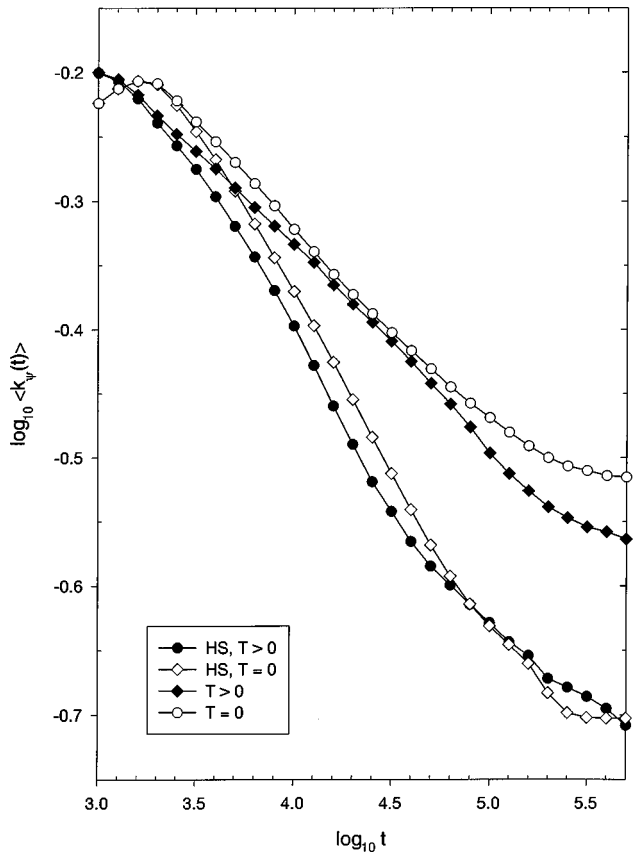

FIG. 17. Time evolution of $\langle k_\psi \rangle$ for a Hele-Shaw cell with thermal fluctuations, a Hele-Shaw cell without thermal fluctuations, an ordinary cell with thermal fluctuations, and an ordinary cell without thermal fluctuations.

$$S_\psi(k) \equiv \frac{1}{N_k} \sum_{\mathbf{k} \in \Delta(k)} S_\psi(\mathbf{k}), \tag{3.10}$$

where $\Delta(k)$ is the circular shell in reciprocal space $\Delta(k) \equiv \{\mathbf{k} | k - \frac{1}{2}\Delta < |\mathbf{k}| < k + \frac{1}{2}\Delta\}$ ($\Delta =$ width of the shell), and N_k is the number of points in the shell. The dynamical scaling hypothesis proposed for phase separation in a binary system [2,5] asserts that there is a single dominant length scale and that the scaled structure factor $F(Q) \equiv \langle k \rangle^2 \hat{S}_\psi(k)$, where $\hat{S}_\psi(k)$ is the normalized $S_\psi(k)$ and $Q \equiv k/\langle k \rangle$ is the scaled wave vector, should be invariant at different times. Figures 12 and 13 plot $F(Q)$ versus Q in the HS cell for $\langle \rho \rangle = 0.1$ and 0.4 [41]. It can be seen clearly that the hypothesis does not hold. There may be more than one dominant length scale in the system. When the average surfactant concentration is lower than the percolation threshold, $F(Q)$ settles down to its asymptotic frozen form in the latter part of the ''algebraic growth regime'' defined by the fits in Fig. 10. If the average surfactant concentration is higher than the threshold, $F(Q)$ does not settle down to an asymptotic frozen form until the growth is frozen, that is, until $t \geqslant 10^{5.3}$. A qualitatively similar behavior is also observed in ordinary cells. This is contrary to what Kawakatsu *et al.* [24] observed in their model, where dynamical scaling behavior was found at all concentrations.

Figures 14 and 15 show the so-called Porod's plots for $\langle \rho \rangle = 0.1$ and 0.4 [41]. Tomita showed clearly in Ref. [42] that the formation of smooth and thin interfaces in d dimensions leads to Porod's law, $\lim_{k \to \infty} k^{d+1} S(k) = \beta_d A$, where $\beta_d = 2^{d-1} \pi^{(d-2)/2} \Gamma(d/2)$ ($\beta_2 = 2$ and $\beta_3 = 2\pi$), and A is the interface area density. Both plots begin to exhibit this asymptotic behavior at $t \approx 10^{4.5}$, indicating the formation of sharp interfaces (cf. the right column in Figs. 1–4). The Porod tail in Figs. 14 and 15 also exhibit a second peak, which was attributed by Shinozaki and Oono to the local curvature fluctuations [33].

D. Joint effect of hydrodynamics and thermal fluctuations

Finally, we present a preliminary investigation of the effect of thermal fluctuations. The CDS scheme used for this investigation is the same as in Eqs. (2.9), except that Eqs. (2.9c) and (2.9d) are replaced by

$$\psi^*(\mathbf{n},t) = \psi(\mathbf{n},t) + M_\psi \tilde{\Delta} \mathcal{I}(\mathbf{n},t) + C_\psi \eta_\psi(\mathbf{n},t)$$

and

$$\rho^*(\mathbf{n},t) = \rho(\mathbf{n},t) + M_\rho \tilde{\Delta} \mathcal{J}(\mathbf{n},t) + C_\rho \eta_\rho(\mathbf{n},t),$$

where the thermal fluctuations $\eta_\psi(\mathbf{n},t)$ and $\eta_\rho(\mathbf{n},t)$ are implemented in the same way as in Refs. [10,43]. Since the C_ψ and C_ρ values used in Ref. [10] lead to numerical overflow when the maximum ($c^2 = 10$) hydrodynamic effect is included, in our simulation we use $C_\psi = C_\rho = 0.01$. Figure 16 shows the time evolution of a Hele-Shaw cell with thermal fluctuations for $\langle \rho \rangle = 0.4$, starting from the same initial distributions of ψ and ρ as in Figs. 3 and 4. As previously observed in Ref. [16], although the domain structure does not show much difference at late times when only hydrodynamics is included, there appears a significant difference when both hydrodynamics and thermal fluctuations are included (cf. Figs. 3, 4, and 16). It can be seen from Fig. 16 that from $t = 2 \times 10^5$ to $t = 5 \times 10^5$ the temporarily trapped surfactants are able to migrate to the interfaces, while at deep quench ($T = 0$) the surfactants are already stuck in domains. Unfortunately, our simulation time is not long enough to see whether all the temporarily trapped surfactants eventually migrate to interfaces at the chosen fluctuation strength C_ψ and C_ρ.

The evolution of the inverse characteristic length $\langle k_\psi \rangle$ is plotted in Fig. 17. It is evident that the thermal fluctuations are irrelevant until a very late stage, as mentioned in Sec. II B. Into this very late stage the thermal fluctuations become relevant because, as discussed in Sec. III A, they become the only force that drives the system away from being frozen. It can be seen that there exists a crossover in the very late stage at which the phase separation shifts from a hydrodynamically driven mechanism to a thermally driven mechanism. Since domains cannot grow infinitely in the presence of surfactants, thermal fluctuations will eventually become incapable of further decreasing $\langle k_\psi \rangle$. By then, what thermal fluctuations can do is simply to reshuffle surfactants and to undulate interfaces. (The time covered in the simulation is too short to see the final stop of domain growth.)

IV. CONCLUSION

Incorporating hydrodynamics into the phase separation dynamics of the model proposed by Komura and Kodama [10] leads to some unexpected results, as presented in Sec. III. The trapping of surfactants in domains of binary fluid at deep quench is an interesting feature that deserves further investigation. For weak thermal fluctuations this feature may be able to survive. For strong thermal fluctuations, although trapping becomes less likely to occur, it will be interesting to study dynamics under the competition of hydrodynamics and thermal fluctuations. Fluid systems with an upper consolute point, when being quenched to low temperature, may be used to examine experimentally the possible existence of trapped surfactant clusters.

The unusual growth behavior observed in our simulations is explained using an estimation of interface tension that is different from the estimation made by Kawakatsu *et al.* [24]. This explanation implies that the algebraic or logarithmic behavior proposed in previous investigations is possibly oversimplified.

[1] T. Ohta, Ann. Phys. (N.Y.) **158**, 31 (1984).
[2] H. Furukawa, Adv. Phys. **34**, 703 (1985).
[3] S. Komura, Phase Transit. **12**, 3 (1988).
[4] G. F. Mazenko, Phys. Rev. B **43**, 8204 (1991).
[5] A. J. Bray, Adv. Phys. **43**, 357 (1994).
[6] G. Gompper and M. Schick, *Self-Assembling Amphiphilic Systems* (Academic, London, 1994) and references therein.
[7] T. Kawakatsu, K. Kawasaki, M. Furusaka, H. Okabayashi, and T. Kanaya, J. Phys.: Condens. Matter **6**, 6385 (1994), and references therein.
[8] D. Chowdhury, J. Phys.: Condens. Matter **6**, 2435 (1994), and references therein.
[9] R. Ahluwalia and S. Puri, J. Phys.: Condens. Matter **8**, 227 (1996), and references therein.
[10] S. Komura and H. Kodama, Phys. Rev. E **55**, 1722 (1997).
[11] J. Melenkevitz and S. H. Javadpour, J. Chem. Phys. **107**, 623 (1997).
[12] F. Mallamace, N. Micali, and S. H. Chen, Physica A **236**, 149 (1997); **235**, 170 (1997).
[13] M. Laradji, H. Guo, M. Grant, and M. J. Zuckermann, J. Phys.: Condens. Matter **4**, 6715 (1992).
[14] H. Kodama and S. Komura, J. Phys. II **7**, 7 (1997).
[15] E. D. Siggia, Phys. Rev. A **20**, 595 (1979).
[16] G. Pätzold and K. Dawson, Phys. Rev. E **52**, 6908 (1995).
[17] S. P. Das and G. F. Mazenko, Phys. Rev. A **34**, 2265 (1986).
[18] H. Lamb, *Hydrodynamics*, 6th ed. (Cambridge University Press, Cambridge, 1932).
[19] G. K. Batchelor, *An Introduction to Fluid Dynamics* (Cambridge University Press, Cambridge, 1967).
[20] A. Shinozaki and Y. Oono, Phys. Rev. A **45**, R2161 (1992).
[21] Y. Oono and S. Puri, Phys. Rev. Lett. **58**, 836 (1987); Phys. Rev. A **38**, 434 (1988).
[22] P.-G. de Gennes and C. Taupin, J. Phys. Chem. **86**, 2294 (1982).
[23] T. Kawakatsu and K. Kawasaki, Physica A **167**, 690 (1990).
[24] T. Kawakatsu, K. Kawasaki, M. Furasaka, H. Okabayashi, and T. Kanaya, J. Chem. Phys. **99**, 8200 (1993).
[25] K. Kawasaki and K. Kawakatsu, Physica A **164**, 549 (1990).
[26] P. C. Hohenberg and B. I. Halperin, Rev. Mod. Phys. **49**, 435 (1977).
[27] For convenience, the surfactant is assumed to have the same density and viscosity as those of the binary fluid.
[28] J. W. Cahn and J. E. Hilliard, J. Chem. Phys. **28**, 258 (1958); J. W. Cahn, *ibid.* **42**, 93 (1965).
[29] H. E. Cook, Acta Metall. **18**, 297 (1970).
[30] S. Puri and Y. Oono, J. Phys. A **21**, L755 (1988); Phys. Rev. A **38**, 1542 (1988).
[31] T. M. Rogers, K. R. Elder, and R. C. Desai, Phys. Rev. B **37**, 9638 (1988).
[32] T. Koga and K. Kawasaki, Phys. Rev. A **44**, R817 (1991); Physica A **196**, 389 (1993).
[33] A. Shinozaki and Y. Oono, Phys. Rev. E **48**, 2622 (1993).
[34] G. Birkhoff, *Hydrodynamics* (Princeton University Press, Princeton, 1960).
[35] M. D. Feit, J. A. Fleck, Jr., and A. Steiger, J. Comput. Phys. **47**, 412 (1982); M. Gruebele, G. Roberts, and A. H. Zewail, Philos. Trans. R. Soc. London, Ser. A **332**, 223 (1990).
[36] Our simulations show that the precise value of the threshold apparently depends on whether or not hydrodynamic effect and thermal fluctuations are present (cf. Fig. 5). It may also depend on the initial distributions of ψ and ρ. For the convenience of discussion, we locate the value to be between 0.2 and 0.3 because in at least one case [Fig. 5(a)], surfactants do not completely coat the domains in the late stage. Nevertheless, our discussion and argument in the following (including the discussion regarding the *early*-stage part of Fig. 9) do not depend on the precise location of the threshold.
[37] K. Kawasaki and T. Ohta, Physica A **118**, 175 (1983).
[38] The recommendation in Sec. IV of Ref. [33] is followed. Averging over six samples for $\langle\rho\rangle = 0.4$ for both ordinary and Hele-Shaw cells gives identical results to these obtained by averaging over two samples. This is consistent with the claim made in Ref. [20] regarding the gross behavior of $\ln\langle k\rangle$.
[39] A fitting is accepted when the square of correlation coefficient is greater than 0.998.
[40] F. P. Buff, R. A. Lovett, and F. H. Stillinger, Phys. Rev. Lett. **15**, 621 (1965); H. W. Diehl, D. M. Kroll, and H. Wanger, Z. Phys. B **36**, 329 (1980).
[41] Following Ref. [33], the scaled wave vector plotted in Figs. 12–15 is defined by $k_w/\langle k\rangle$, where
$$k_w(k) \equiv \frac{1}{N_k} \sum_{\mathbf{k} \in \Delta(k)} |\mathbf{k}|.$$
[42] H. Tomita, Prog. Theor. Phys. **72**, 656 (1984); **75**, 482 (1986).
[43] S. Puri and Y. Oono, J. Phys. A **21**, L755 (1988).